

# We are IntechOpen, the world's leading publisher of Open Access books Built by scientists, for scientists

6,900

Open access books available

186,000

International authors and editors

200M

Downloads

Our authors are among the

154

Countries delivered to

TOP 1%

most cited scientists

12.2%

Contributors from top 500 universities



WEB OF SCIENCE™

Selection of our books indexed in the Book Citation Index  
in Web of Science™ Core Collection (BKCI)

Interested in publishing with us?  
Contact [book.department@intechopen.com](mailto:book.department@intechopen.com)

Numbers displayed above are based on latest data collected.  
For more information visit [www.intechopen.com](http://www.intechopen.com)



---

# Equal Frequency Surface

---

G. Alagappan

Additional information is available at the end of the chapter

<http://dx.doi.org/10.5772/59887>

---

## 1. Introduction

A photonic crystal (PC) forbids propagation of light in a spectral range called photonic band gap. Within this frequency gap, PC behaves like an insulator for light. The insulating properties of the PC have been widely used in the developments of waveguides, fibers and cavities. For frequencies outside the photonic band gaps though light can propagate, the propagation properties (i.e. conducting properties) are uniquely different. The distinct conducting properties of the PC have led to discoveries of novel functionalities such as superprism effects, large angle polarization splitting, negative refraction, and superlensing.

The conducting properties of a PC can be best – analyzed using an equal frequency surface (EFS). The EFS is a surface in a three-dimensional (3D) PC, and a contour in a 2D PC. The gradient of the EFS plays a key role in determining the group velocity direction and hence, the propagation direction of light in the PC. Important developments on the EFS analysis for PCs can be found in [1-7].

EFS is typically obtained using a plane wave expansion methodology [8-9]. If the dielectric contrast of the PC is large, then a large number of plane waves is required to obtain EFSs with good accuracy. However, the distinct conducting properties, like superprism and beam splitting are normally well-pronounced in the PCs with a small dielectric modulation. [10-13]. For such PCs with small dielectric modulation, the requirement on the large number of plane waves to obtain the EFS can be relaxed.

In this chapter we will outline the theory of the EFS construction, and their applications in determining the conducting properties. For the sake of an easy understanding, throughout this chapter, we will use 2D PCs for illustrations and discussions. The chapter is organized as follows. The second section of the chapter focuses on the exact and approximate constructions of EFSs. Specifically, using one and two plane waves approximations [5], simple and handy analytical expressions for EFSs will be shown. It is worth mentioning that in the electronic

energy band theory, the one plane wave technique is used to approximate Fermi surfaces of a metal, and it is known in the name of Harrison's principles [14-15]. In the third section, we will outline a graphical technique that uses EFSs to determine light propagation directions in the PC. Fourth section of the chapter elaborates on the applications of the EFSs. Particularly, we show the usage of the EFSs to describe superprism, effective negative refractive index mediums, negative refractions, and superlens phenomena in PCs. Finally, fifth section of the chapter gives a summary of the whole chapter.

## 2. EFS construction

In order to construct an EFS for a specific frequency, firstly, a photonic band structure has to be calculated. The photonic band structure can be calculated using a plane wave expansion method. For the details of this method, see [8-9]. The photonic band structure should contain frequencies for a dense number wavevectors in the first Brillouin zone (BZ). For a 2D PC, the EFS can be obtained by projecting the 2D photonic band structure onto the wavevector plane  $(k_x, k_y)$ , keeping a constant frequency.

In a homogenous dielectric medium of refractive index  $n$ , the dispersion relation is  $\omega = ck/n$ , where  $\omega$ ,  $c$ , and  $k$  are the angular frequency, speed of light, and wavevector, respectively. In 2D, the dispersion relation is  $\omega^2 = c^2(k_x^2 + k_y^2)/n^2$ . Thus, as shown in Figure 1, the EFSs of a homogeneous dielectric medium are circles. In a PC, the dispersion relation (i.e., the photonic band structure) is complicated, and therefore EFSs have to be calculated numerically.

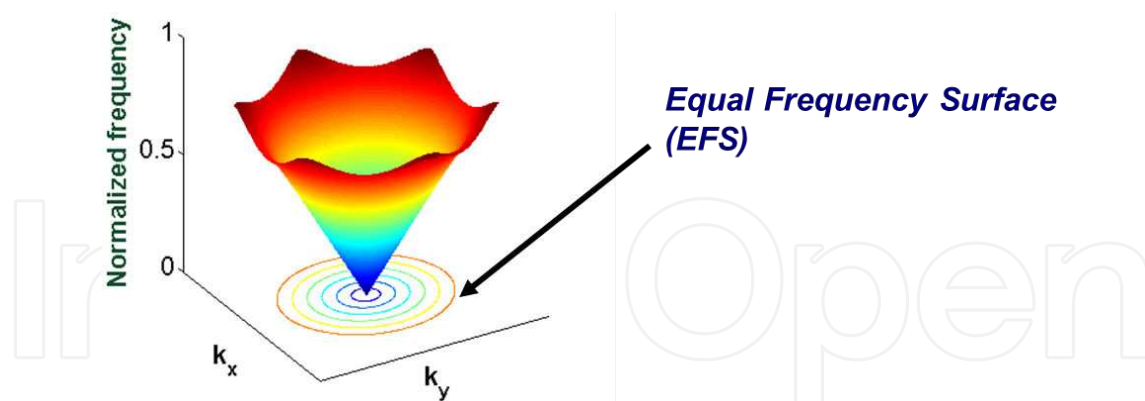


**Figure 1.** photonic band structure, and EFSs of a homogenous dielectric medium

Let's take examples of EFSs in a 2D square lattice PC made of circular silicon rods (dielectric constant=12.1) in an air matrix (dielectric constant=1.0). In such a system, the two polarizations of light can be decoupled. The band structure of the  $E$  – polarization (electric field perpendicular to the 2D periodic plane) is shown in Figure 2, for a silicon rod radius of 0.2. The vertical axis in this figure represents the normalized frequency,  $\omega = a/\lambda$ , with  $a$  and  $\lambda$  being the period and free space wavelength, respectively. As we can see from the 2D band structure, in the long

wavelength limit (i.e.,  $a \ll \lambda$ ), the dispersion relationship is similar to a homogenous medium (Fig. 1).

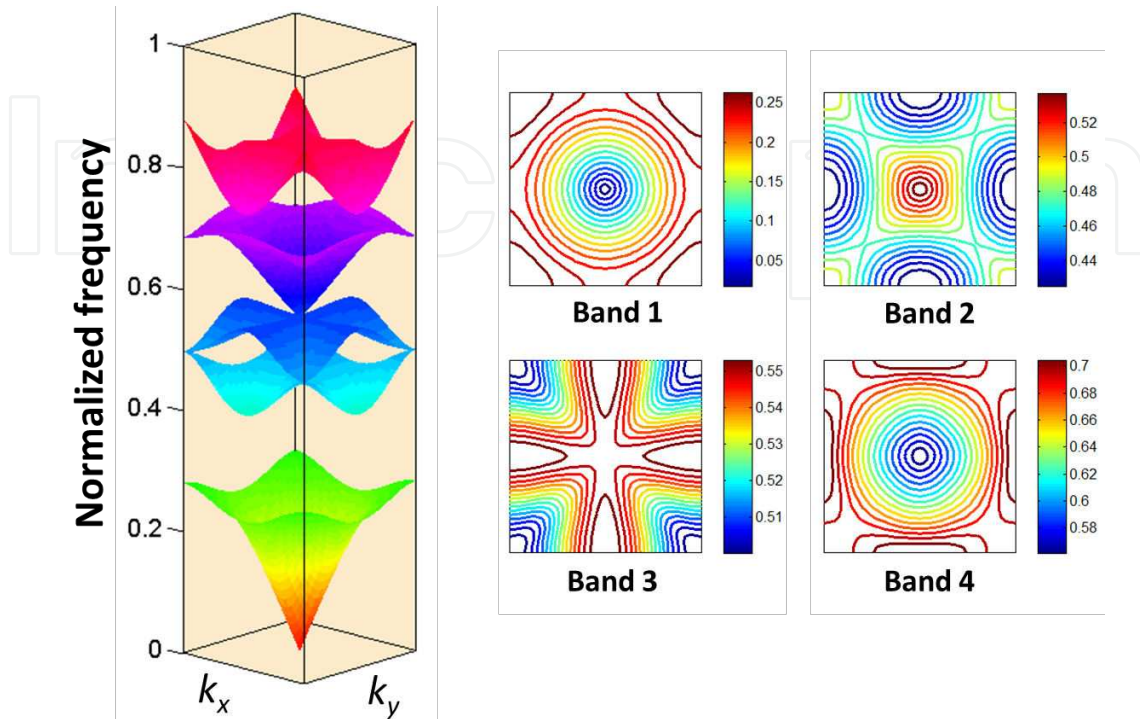


**Figure 2.** Photonic band structure in 2D and EFSs (in 2D these are constant frequency contours) of a 2D PC [circular silicon rods with a radius of 0.2, air matrix]. The color bars indicate the normalized frequencies

### 2.1. Approximation techniques

In a 3D PC made of either isotropic or anisotropic materials, it is known that the Maxwell equations corresponding to two independent polarizations of light are coupled [9,16-17]. For a 2D PC made of isotropic materials, we can always decouple the equations into two independent equations, corresponding to the two independent polarizations [9, 16]. On the other hand, for a 2D PC made of an anisotropic material, such a decoupling of polarizations is not possible in general. However, by restricting one of the principal axes of the anisotropic material to be perpendicular to the periodic plane of the 2D PC and the other two principal axes residing in the periodic plane, decoupling is possible [6,18-20]. Detail mathematical treatment of the polarization decoupling in a 2D PC made of anisotropic materials can be found in [6].

Assuming the polarizations can be decoupled, the photonic band structure of the  $H$ -polarization (magnetic field perpendicular to the periodic plane) or the  $E$ -polarization can be found by solving the differential-equation in the form [9,6,16],

$$\hat{D}[\mathbf{H}(\mathbf{r})] = (2\pi\omega / a)^2[\mathbf{H}(\mathbf{r})], \tag{1}$$

for a given wavevector in the first BZ. In Eqn. 1,  $\mathbf{H}(\mathbf{r})$  is the position ( $\mathbf{r}$ ) dependent magnetic field vector, and  $\hat{D}$  is a differential operator that depends on the polarization, and the dielectric constant profile of the PC. Using the plane wave expansion method [9,6-7,16], we can transform Eqn. 1 to a matrix eigen-value problem. Consequently, the frequency containing term  $(2\pi\omega/a)^2 = \Omega$  in Eqn. 1, can be written as a matrix vector product,

$$\Omega = \mathbf{h} \cdot \hat{M} \mathbf{h}. \quad (2)$$

In this equation,  $\mathbf{h} = [h_1, h_2, \dots]'$ , where  $h_n$  is the Fourier expansion coefficient of  $\mathbf{H}(\mathbf{r})$  associated with the reciprocal lattice vector  $\mathbf{G}_n$ . The matrix element of  $M$  [6] is defined as

$$M_{mn} = \begin{cases} \langle k_m | \tilde{\beta}_r(m-n) | k_n \rangle, & H\text{-polarization} \\ |k_m| |k_n| \beta(m-n), & E\text{-polarization} \end{cases} \quad (3)$$

Here  $|k_n\rangle = \mathbf{k} - \mathbf{G}_n$ , with  $\mathbf{k} = [k_x, k_y]'$ . In Eqn. 3,  $\langle \dots \rangle$  represents the inner product of the vector, matrix and vector. For the  $H$ -polarization,  $\tilde{\beta}_r(n)$  is the 2 by 2 matrix defining the inverse Fourier transform coefficient of the tensor dielectric function [associated with  $\mathbf{G}_n$ ], and similarly for the  $E$ -polarization,  $\beta(n)$  is the inverse Fourier transform coefficient of the scalar dielectric function.

Eqn. 2 defines an EFS for a given frequency, and has to be evaluated using the entire basis of the reciprocal space, which is infinite in number. In practice, the number of basis (i.e. the number of plane waves) is limited to a number for which the corresponding result achieves a required degree of accuracy. In general, larger the dielectric modulation, larger the number of required plane waves. For PCs with weak dielectric modulations, the number of plane waves can be significantly less. In the following sections, we will use one and two plane waves to approximate the EFS of the weakly modulated PCs, and as we shall see, such approximations lead to handy analytical expressions.

### 2.1.1. One plane wave approximation

Firstly, we will elaborate the one plane wave approximation [5] for the  $H$ -polarization. Consider a 2D PC made of two materials with permittivity tensors  $\tilde{\epsilon}_a$  and  $\tilde{\epsilon}_b$ , and assume the fill factor of the material with the permittivity tensor  $\tilde{\epsilon}_a$  is  $f$ . The one plane wave technique assumes a very weak dielectric modulation such that  $\tilde{\beta}_r(m-n)$ , can be approximated with only one plane wave (i.e., one Fourier component) as  $\tilde{\beta}_r(m-n) = \delta_{mn} \tilde{\epsilon}_0^{-1}$ , where  $\tilde{\epsilon}_0$  is the averaged dielectric tensor,

$$\tilde{\epsilon}_0 = \tilde{\epsilon}_a f + (1-f) \tilde{\epsilon}_b. \quad (4)$$

Using this assumption, and  $h=[0.. 1.. 0]'$  with 1 at the  $m$ -th position [Eqn. 2], we can show that,

$$\Omega = \langle k_m | \tilde{\varepsilon}_0^{-1} | k_m \rangle. \quad (5)$$

Eqn. 4 has to be true for every integer  $m$ . The tensor  $\tilde{\varepsilon}_0$  in general can be written as  $\tilde{\varepsilon}_0 = Q^T \tilde{\varepsilon}_p Q$  [6], where  $\tilde{\varepsilon}_p$  is the dielectric tensor of the anisotropic material in its principal coordinate system,  $Q$  is a rotational operator (an orthogonal operator), and  $Q^T$  is the transpose of  $Q$ . With this  $\tilde{\varepsilon}_0$ , Eqn. 5 can be rewritten using the inner product properties [21] to,

$$\Omega = \langle k_m | Q^T \tilde{\varepsilon}_p^{-1} Q | k_m \rangle = \langle Q k_m | \tilde{\varepsilon}_p^{-1} | Q k_m \rangle, \quad (6)$$

where  $Q | k_m \rangle = \mathbf{k}' - \mathbf{G}'_m = [k_{x'} - G_{mx'}, k_{y'} - G_{my}]'$  is the rotated vector of  $| k_m \rangle = \mathbf{k} - \mathbf{G}_m = [k_x - G_{mx}, k_y - G_{my}]'$ . If one of the material is assumed to be isotropic, and the other is assumed to be anisotropic which is often the case [6,19], then using Eqn. 4 we have,

$$\tilde{\varepsilon}_p^{-1} = \begin{pmatrix} 1 / \{ \varepsilon_a f + \varepsilon_{b1} [1 - f] \} & 0 \\ 0 & 1 / \{ \varepsilon_a f + \varepsilon_{b2} [1 - f] \} \end{pmatrix}, \quad (7)$$

where  $\tilde{\varepsilon}_a$  is taken as an identity matrix multiplied by a constant,  $\varepsilon_a = n_a^2$  (i.e., an isotropic material) and  $\tilde{\varepsilon}_b$  is assumed as the dielectric tensor of the anisotropic material in the principal coordinate system, with  $\varepsilon_{b1}$  and  $\varepsilon_{b2}$  being the principal dielectric constants. Substituting the expressions for  $Q | k_m \rangle$  and  $\tilde{\varepsilon}_p^{-1}$  in Eqn. 6, we obtain the following equation for the EFS of the  $H$ -polarization in the rotated frame,

$$\frac{(k_{x'} - G_{mx'})^2}{\varepsilon_a f + \varepsilon_{b1} [1 - f]} + \frac{(k_{y'} - G_{my'})^2}{\varepsilon_a f + \varepsilon_{b2} [1 - f]} = \Omega. \quad (8)$$

Eqn. 8 describes an ellipse in the rotated frame  $(k_{x'}, k_{y'})$  with the origin at  $\mathbf{G}'_m = [G_{mx'}, G_{my}]'$ . As the equation is true for every  $m$ , there will be repetitions of the same ellipse for each  $m$  [corresponding to each reciprocal lattice vector].

Similarly, for the  $E$ -polarization, it can be shown that, the one plane wave approximation leads to  $|k_m|^2 = \Omega \varepsilon_0$ , where  $\beta(m - n) = \delta_{mn} / \varepsilon_0$  has been used for Eqn. 3. Assuming  $|k_m \rangle = \mathbf{k} - \mathbf{G}_m$ , we will arrive at the same equation as Eqn. 8, however the denominators at the left hand side of the Eqn. 8 are replaced with  $\varepsilon_0 = \varepsilon_a f + \varepsilon_{b3} (1 - f)$ . Here,  $\varepsilon_{b3}$  is the principal dielectric constant of the anisotropic material experienced by the  $E$ -polarization. Note that for the  $E$ -polarization Eqn. 8 describes a circle.

To illustrate the EFS construction, let's first assume both materials are isotropic (i.e.  $\epsilon_{b1}=\epsilon_{b2}=\epsilon_{b3}=n_b^2$ ) and consider a 2D PC with a square lattice,  $n_a=1.6$ ,  $f=0.4$ , and a very small dielectric modulation (i.e.  $n_a \approx n_b$ ). Note that, with isotropic materials, and very small dielectric modulation, the distinction between the EFSs of  $E$  and  $H$  – polarizations vanishes.

For an instance of the EFS construction, consider  $\omega=0.5$ . Using the radius given by Eqn. 8, let's draw circles at each reciprocal lattice point as shown in Figure 3(a). Each closed contour constitutes to an EFS of a particular band. The bands are indexed according to their positions in the extended zone diagram [14-15].

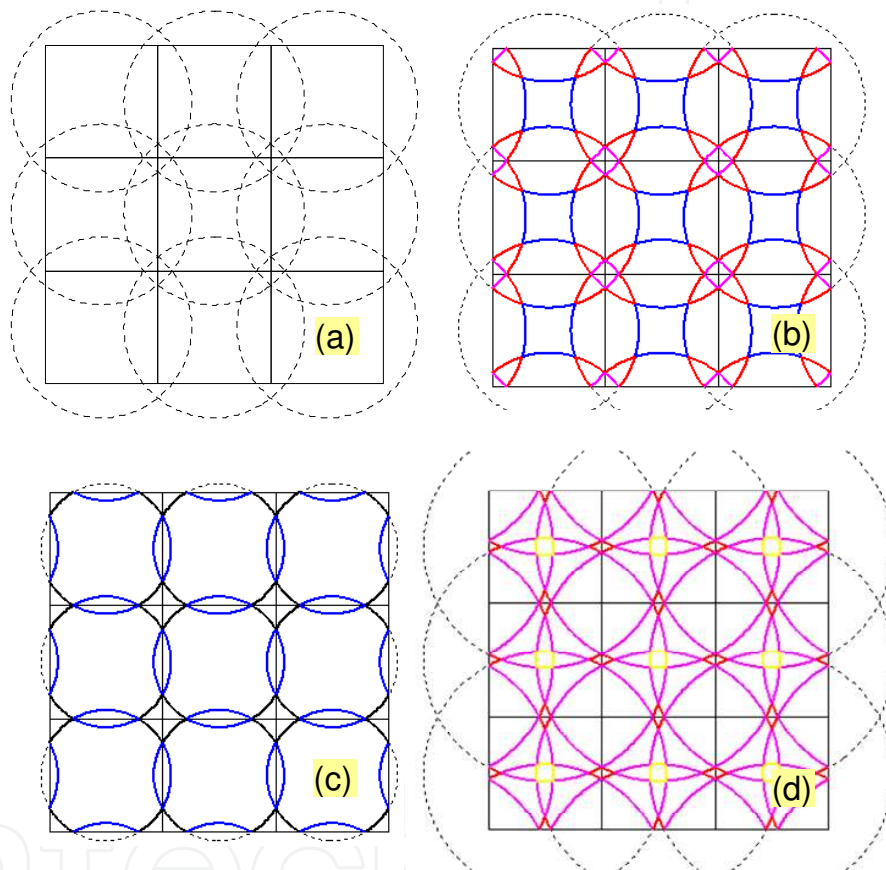


**Figure 3.** EFS constructions of a square lattice PC with  $f=0.4$ ,  $n_a = 1.6$  and  $n_a \approx n_b$ . Band indices: band 1 – black, band 2 – blue, band 3 – red, band 4 – pink, band 5 – yellow. The square boxes indicate boundaries of the BZs (a) EFS construction for  $\omega=0.5$  (b) EFS for  $\omega=0.5$  (c) EFS for  $\omega=0.36$  (d) EFS for  $\omega=0.67$ .

Now let's demonstrate the validity of the EFS obtained from the one plane wave approximation, by comparing it with the numerically evaluated. In Figures 4(a) and 4(b), we plot EFSs ( $\omega=0.5$ ) for  $n_b=2.0$  and  $2.6$ , respectively, and all other parameters are kept the same as in Fig. 3. The one plane wave construction is shown in the black dashed lines, whereas the EFS obtained from the numerical calculation is highlighted in color. As it is clear from Fig. 4(a), for the PC with weak dielectric modulation (i.e.,  $n_b=2.0$ ), the one plane wave construction agrees well with the numerically calculated EFS. However, when the dielectric modulation increases,

the degree of disagreement increases (Fig. 4(b)). Nevertheless, in PCs with large dielectric modulations, one plane wave approximation still can be used to gain a rough idea on the EFSs shapes, for frequencies far from the photonic band edge. It is important to note that one or two plane wave approximations (discussed in Sec. 2.1.2) fail when the frequency is close to the photonic band edge (see Fig. 14; Sec. 4.2; and [2]).

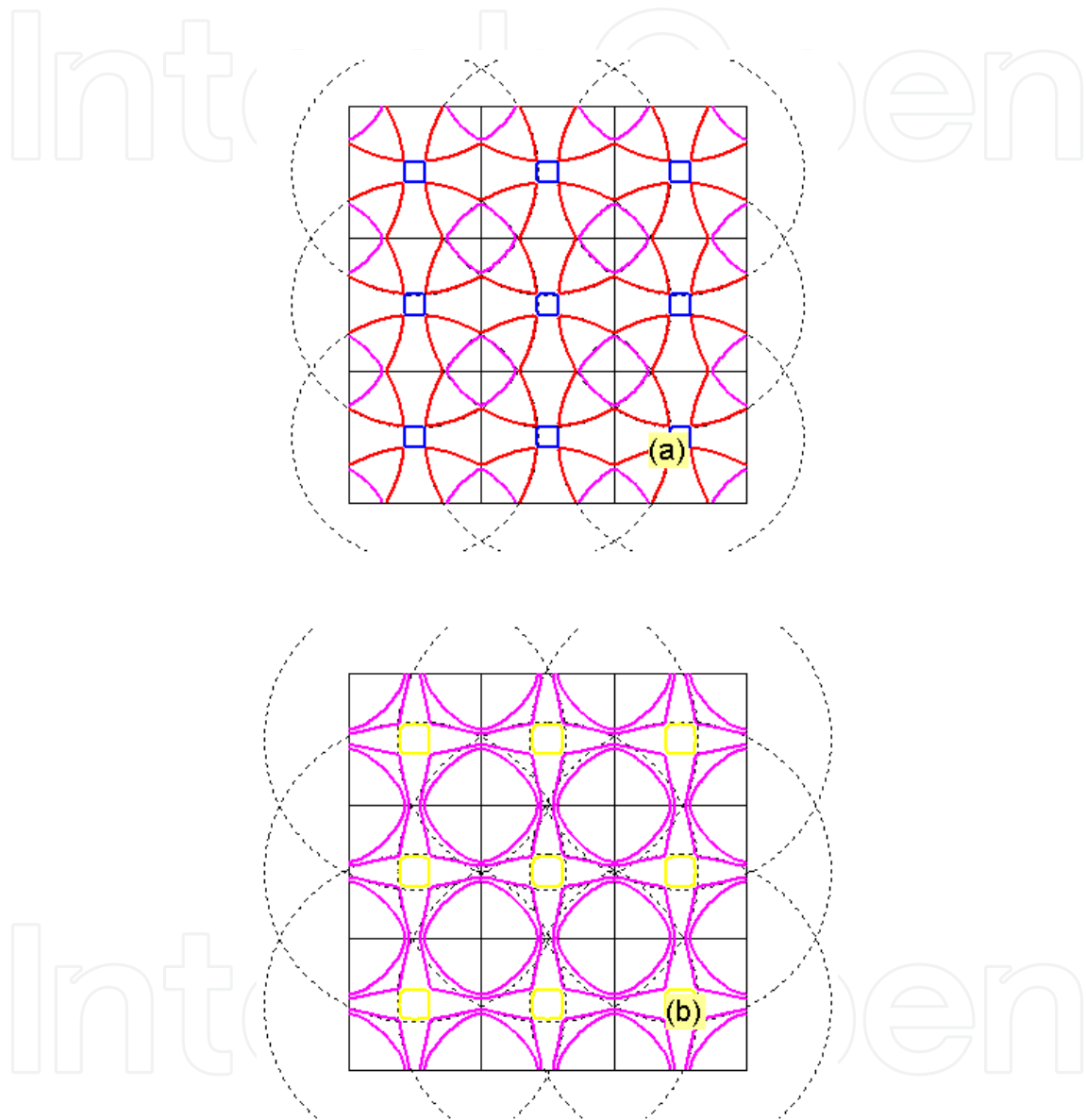


**Figure 4.** EFS constructions (dashed black line) and the numerically calculated EFS (color) of a square lattice PC with  $f=0.4$ ,  $n_a=1.6$ , and  $\omega=0.5$ . Band indices: band 3 – red, band 4 – pink, band 5 – yellow. (a) EFS for  $n_b=2.0$  (b) EFS for  $n_b=2.6$

Finally, we provide an EFS construction example for a 2D PC made of an anisotropic material. Consider a square lattice PC with an anisotropic material ( $\sqrt{\epsilon_{b1}}=1.6$ ,  $\sqrt{\epsilon_{b2}}=2.0$ ),  $n_a=1.8$ , and  $f=0.2$ . The principal axis with the dielectric constant  $\epsilon_{b1}$  is oriented  $45^\circ$  with respect to the  $k_x$  – axis of the PC, as shown Figure 5(a). The  $Q$  operator in Eqn. 6 is a  $45^\circ$  anticlockwise rotational operator.

Hence, based on Eqns. 6 – 8, we draw ellipse at each reciprocal lattice point in the rotated coordinate system as shown in Fig. 5(a). The numerically calculated EFS for the  $H$ -polarization with  $\omega=0.5$  is shown in Fig. 5(b), and as we can readily verify from the figure, both the construction and numerical evaluation share a good agreement.

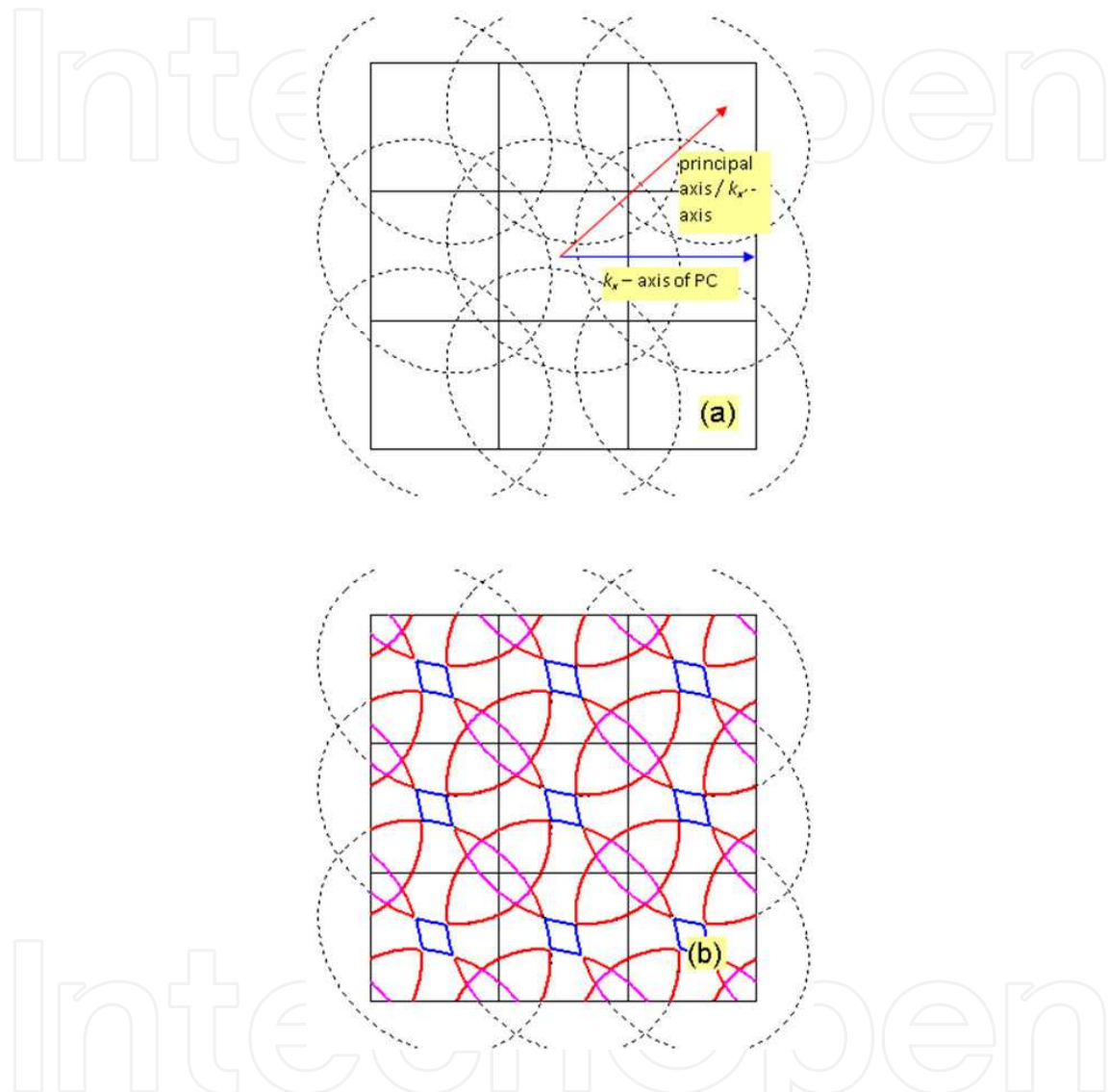


**Figure 5.** EFS construction [ $\omega=0.5$ ] for the  $H$ -polarization (dashed black line), and the numerically calculated EFS (color) of a square lattice PC with an anisotropic material ( $f=0.2, n_a=1.8, \sqrt{\epsilon_{b1}}=1.6, \sqrt{\epsilon_{b2}}=2.0$ ). Band indices: band 2 – blue, band 3 – red, band 4 – pink. (a) EFS construction (b) EFS with the band index assignment.

### 2.1.2. Two plane wave approximation

Although, one plane wave approximation seems to be good in approximating the EFS of a 2D PC with a weak dielectric modulation, a magnified version of the one plane wave EFS, will show that this approach is unable to approximate the edges of the EFS accurately. This problem can be addressed by using two plane waves approximation.

For the sake of simplicity, we will demonstrate the two plane waves approximation for 2D PCs made of isotropic materials. We will further assume the dielectric modulation is finite and weak, such that only two Fourier coefficients of  $\beta(i)$ ,  $\beta(0)$  and  $\beta(1)$ , are significant. With these, we can approximate Eqn. 2 as,

$$\Omega = h_i M_{i,i} h_i + h_i M_{i,i+1} h_{i+1} + h_{i+1} M_{i+1,i} h_i + h_{i+1} M_{i+1,i+1} h_{i+1}, \quad (9)$$

which has to be true for every  $i$ . We can choose  $i=1$ , and the eigenvalues of the resulting  $M$ , can be obtained by finding the determinant of the matrix,

$$\begin{bmatrix} M_{11} - \Omega & M_{12} \\ M_{21} & M_{22} - \Omega \end{bmatrix}. \quad (10)$$

Using the fact  $M_{ij}=M_{ji}$ , and denoting  $\beta(i)$  as  $\beta_i$ , we can show,

$$2\Omega = \beta_0(k_0^2 + k_1^2) \pm \sqrt{\beta_0^2(k_0^2 - k_1^2)^2 + (2\beta_1 k_0 k_1)^2}, \quad (11)$$

where  $k_i k_j$  represents  $\langle k_i | k_j \rangle$  and  $|k_i| |k_j|$  for the  $H$ - and  $E$ -polarizations, respectively. Note that for a weak dielectric modulation,  $\beta_0 \gg |\beta_1|$  and  $\beta_0 > 0$ .

Eqn. 11 can be evaluated using specific choices of wavevectors and reciprocal lattice vectors. For an instance, let's examine EFSs near the first band gap of the  $E$ -polarization, in the square lattice PC around the  $X(-\pi/a, 0)$  point. With  $g=2\pi/a$ ,  $\mathbf{k}=[k_x k_y]'$ ,  $\mathbf{G}_0=[0 0]'$ , and  $\mathbf{G}_1=[-g 0]'$ , the terms in Eqn. 11 become,

$$\begin{aligned} \beta_0(k_0^2 + k_1^2) &= 2\beta_0[(k_x + g/2)^2 + k_y^2 + g^2/4] \\ \beta_0^2(k_0^2 - k_1^2)^2 &= [2\beta_0 g(k_x + g/2)]^2 \\ (2\beta_1 k_0 k_1)^2 &= 4\beta_1^2[(k_x + g/2)^2 + k_y^2 + g^2/4]^2 - [2\beta_1(k_x + g/2)]^2. \end{aligned} \quad (12)$$

Let's move the origin of the reciprocal space from  $(0,0)$  to the  $X$  point, by writing  $k_x=k_x+g/2$ . In the new coordinate system, using Eqns. 11 and 12, we can show that,

$$\Omega = \beta_0(k_x^2 + k_y^2 + g^2/4) \pm \sqrt{(\beta_0 k_x g)^2 + \beta_1^2(k_x^2 + k_y^2 + g^2/4)^2 - (\beta_1 k_x g)^2}. \quad (13)$$

Eqn. 13 does not provide any insight to the shape of the EFS. More useful information can be obtained if we can transform the equation to a simpler form. To do this, we first seek an approximation to the square root term in Eqn. 13, for a small  $k_x$ . For a small  $k_x$ , the square root term in Eqn. 13, can be written as  $y = \sqrt{P^2 + Q^2}$ , where  $P = |\beta_0 k_x g|$  and  $Q = \beta_1(k_x^2 + k_y^2 + g^2/4)$  (the term  $\beta_1 k_x g$  in Eqn. 13 is neglected). We can approximate  $y$  using a binomial expansion as  $\approx Q + \frac{P^2}{2Q}$ . However, this requires  $Q \gg P$ , and in fact this is a good assumption as we shall justify later in the discussion. Using the binomial expansion of  $y$ , for a small  $k_x$  and  $k_y$ , Eqn. 13 can be simplified to,

$$\left[ \Omega_1 - \frac{g^2}{4}(\beta_0 - |\beta_1|) \right] = k_x^2 \left( \beta_0 - |\beta_1| - \frac{2\beta_0^2}{|\beta_1|} \right) + k_y^2 (\beta_0 - |\beta_1|), \quad (14)$$

$$\left[ \Omega_2 - \frac{g^2}{4}(\beta_0 + |\beta_1|) \right] = k_x^2 \left( \beta_0 + |\beta_1| + \frac{2\beta_0^2}{|\beta_1|} \right) + k_y^2 (\beta_0 + |\beta_1|), \quad (15)$$

where the two solutions of Eqn. 13 are denoted as  $\Omega_1$  and  $\Omega_2$ . These two solutions correspond to frequencies in band 1 [ $\Omega_1$ ] and band 2 [ $\Omega_2$ ]. With  $\beta_0 > 0$  and  $\beta_0 > |\beta_1|$ , we have  $\beta_0 + |\beta_1| + \frac{2\beta_0^2}{|\beta_1|} > 0$ , in Eqn. 15. Therefore, EFSs for band 2 are elliptical (provided that  $Q \gg P$ ) with the lengths of the semi-major and -minor proportional to the reciprocals of  $\sqrt{\beta_0 + |\beta_1| + \frac{2\beta_0^2}{|\beta_1|}}$  and  $\sqrt{\beta_0 + |\beta_1|}$ , respectively. On the other hand, note that, the EFSs for band 1 (Eqn. 14, with  $\beta_0 - |\beta_1| - \frac{2\beta_0^2}{|\beta_1|} < 0$ ) are not elliptical.

Now let's examine the validity of the assumption  $Q > P$  in deriving Eqns. 14 and 15. The expressions  $P$  and  $Q$  are linear and quadratic functions of  $k_x$ , respectively, and the minimum point of  $Q$  is  $f(k_y) = |\beta_1| \left( k_y^2 + \frac{g^2}{4} \right)$ . Hence, a sufficient condition for  $Q > P$  is simply  $f(k_y) > P$ . Inserting the expression for  $P$ , this condition becomes,

$$-\frac{|\beta_1|}{\beta_0 g} \left( k_y^2 + \frac{g^2}{4} \right) < k_x < \frac{|\beta_1|}{\beta_0 g} \left( k_y^2 + \frac{g^2}{4} \right)$$

The conditions on  $k_y$  can be obtained by solving the quadratic in-equality  $Q - P > 0$ . Solving this in-equality, we have,

$$k_y > \frac{g}{2|\beta_1|} \sqrt{\beta_0^2 - \beta_1^2}.$$

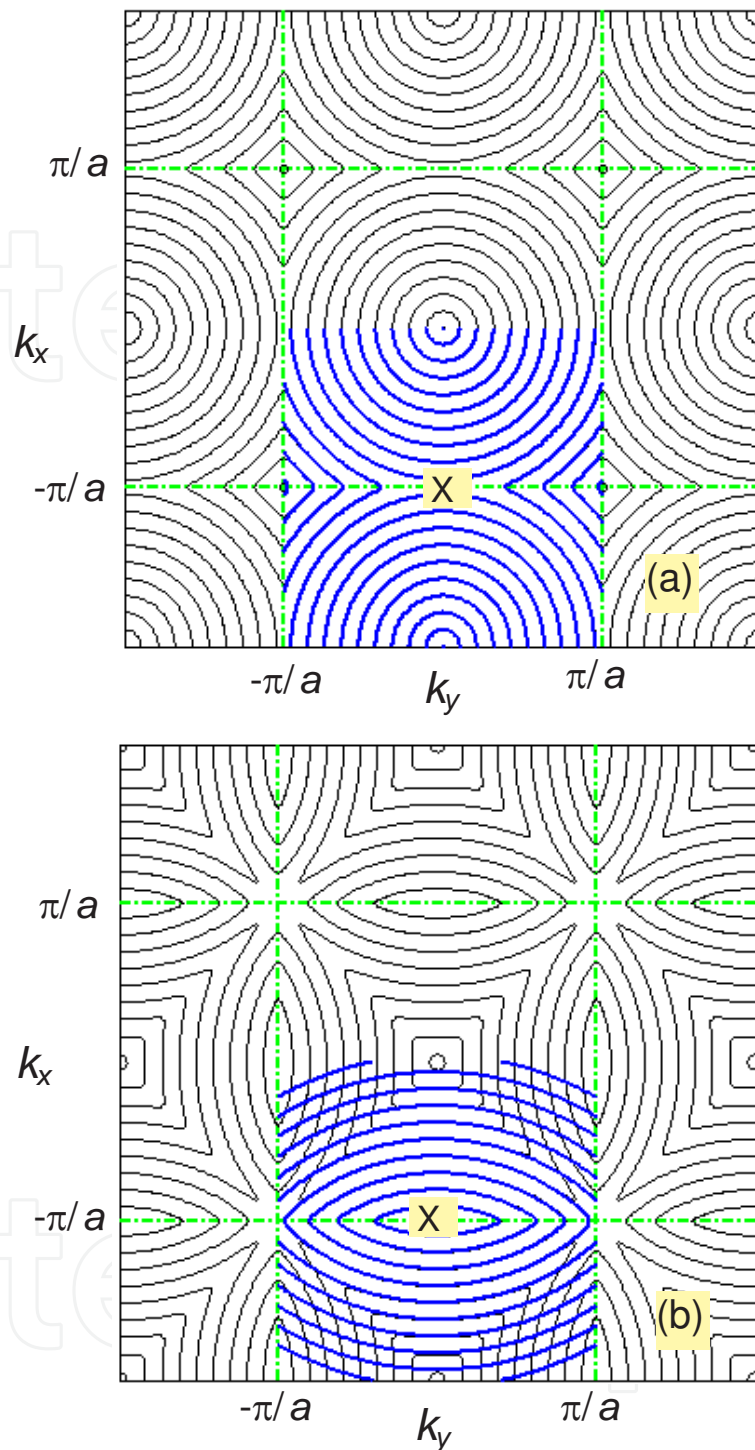


**Figure 6.** EFS approximations using two plane waves approximation [square lattice PC with  $n_a=1.6$ ,  $n_b=1.8$ , and  $f=0.2$ ]. The numerically calculated EFS (thin black lines) and the approximated EFS (thick blue lines) for frequencies in the (a) first band (b) second band.

To illustrate the EFS construction using the two plane waves approximation, consider a square lattice PC with  $n_a=1.6$ ,  $n_b=1.8$ , and  $f=0.2$ . The numerically calculated EFS and the approximated EFS, for frequencies in the first and the second band are shown in Figures 6(a) and 6(b),

respectively. In both figures, we have evaluated Eqn. 11 for  $-\pi/a < k_y < -\pi/a$  and  $-2\pi/a < k_x < 0$ , and the results share a good agreement with those of numerical evaluation. As Eqn. 9 has to be true for every  $i$ , we can translate the EFS approximated for  $i=1$  by a vector  $\mathbf{G}_i$ . Furthermore the EFSs in the neighborhood at the other symmetrical X points [i.e.  $(\pi/a, 0)$ ,  $(0, \pi/a)$  and  $(0, -\pi/a)$ ] can be obtained using the EFS approximated in the neighborhood of  $X(-\pi/a, 0)$  by point group – symmetry operations [9, 22].

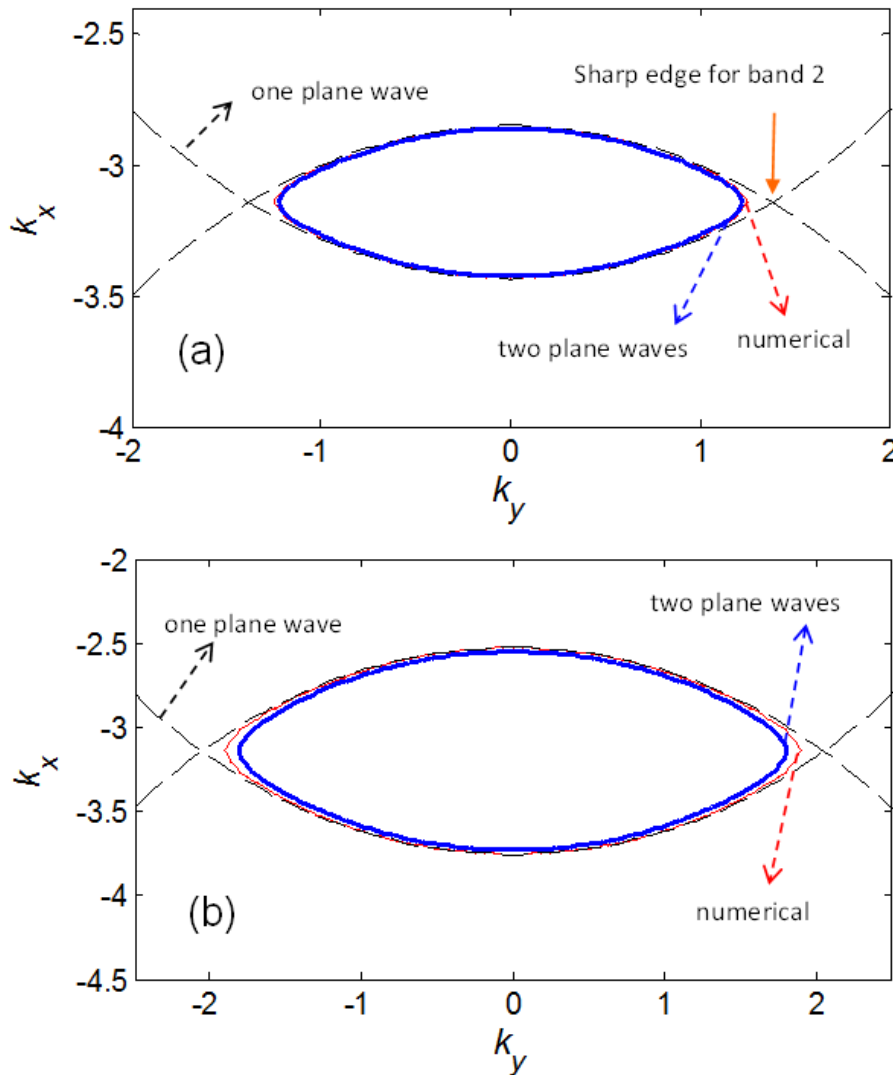


**Figure 7.** The merit of the two plane waves approximation. EFSs for a square lattice PC with  $n_a=1.6$ ,  $f=0.2$ . EFS ( $\omega=0.31$ ) obtained from the one plane wave approximation (dashed black line), two plane waves approximation (thick blue line), and the numerical calculation (thin red line), for (a)  $n_b=1.8$  (b)  $n_b=2.0$ . Both  $k_x$  and  $k_y$  in (a) and (b) have units of  $1/a$ .

In order to appreciate the ability and inability of the two plane waves approximation, we plot EFSs (band 2,  $\omega=0.3$ ) obtained from the one plane wave approximation, two plane waves approximation, and the full numerical calculation in Figures 7(a) and 7(b), for  $n_b=1.8$  and  $n_b=2.0$ , respectively. The one plane wave – EFS is constructed using two circles originated from  $(0,0)$  and  $(-g, 0)$  points. Thus, it always predicts sharp edges for the EFS (see band 2 in Figs. 3(c), 7(a)

and 7(b)). The sharp edges does not appear in the numerically calculated EFS, which is the accurate EFS. The failure of the one plane wave method is corrected in the two plane waves approximation. The two plane waves approximation perfectly matches the numerical counterpart when the dielectric modulation is small (Fig. 7(a)). As expected, when the dielectric modulation becomes large, the two plane waves approximation becomes poorer (Fig. 7(b)), however the approach still exhibits a better accuracy compared to the one plane wave approach.

### 3. Propagation directions

When light crosses the boundary between two homogenous mediums (medium 1 and medium 2), light refracts. The light in medium 1 with an incident angle,  $\theta_i$ , can excite two symmetrical waves (with angles  $\theta_p$ ; see Figure 8) in medium 2. What happens to this refraction picture, when we replace the homogenous dielectric medium 2, with a PC? When we replace the homogenous medium 2, with a PC, the simple refraction picture based on the Snell's law will disappear. A more general technique has to be used, in order to find light propagation directions. This section reviews the well – known method [1-4] of finding light propagation directions in PCs, based on their EFS. As a pre-requisite for the second part in this section, we will first give a brief review on anisotropic PCs [22].

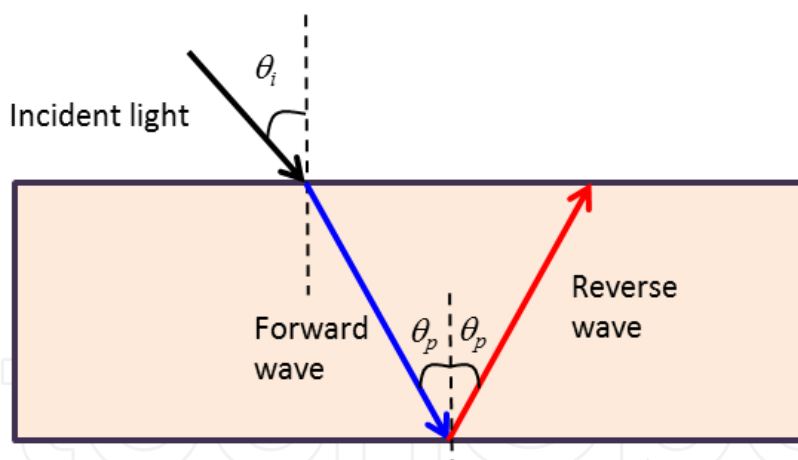


Figure 8. Light propagation from a homogenous dielectric medium 1 to a homogenous dielectric medium 2

#### 3.1. Orientation parameter – Anisotropic PC

A PC may be simply viewed as a lattice with a motif attached to each lattice point. If the re-orientation of the motif causes the symmetry elements of the PC to change, then the corresponding PC is an anisotropic PC, as opposed to an isotropic PC, where the orientation of the motif is irrelevant to the symmetry of the PC. A 2D PC made of only isotropic dielectric materials, with a circular motif in a 2D lattice, is a clear example of a 2D isotropic PC. Aniso-

tropic PCs, on the other hand, can be geometrically anisotropic or materially anisotropic. Figure 9(a) shows the geometry of a 2D hexagonal lattice PC with a square motif. The orientation of the square motif with respect to the underlying lattice plays a crucial role in determining the optical properties of the 2D PC. In Fig. 9(b), instead of a square motif, we have a circular motif for which the corresponding orientation is irrelevant. If all materials are isotropic, then the geometries in Figs. 9(a) and 9(b) represent examples of geometrically anisotropic and isotropic PCs, respectively. In the presence of an anisotropic material, the optical properties of the PC will vary in accordance to the orientation of the anisotropic material (i.e., the orientation of the principal axes with respect to the lattice), and therefore the corresponding PC is defined as a materially anisotropic PC. A PC with a geometry in Fig. 9(b) constitutes to a materially anisotropic PC, if either the matrix or the circular cylinder is an anisotropic medium. On the other hand, in the presence of an anisotropic material, a PC with a geometry as shown in Fig. 9(a) has a mixed anisotropy (i.e., both geometrical and material's anisotropy exist).

As we will show in the next section, the orientation parameter of the anisotropic PC is crucial, as to determine the accurate light propagation direction.

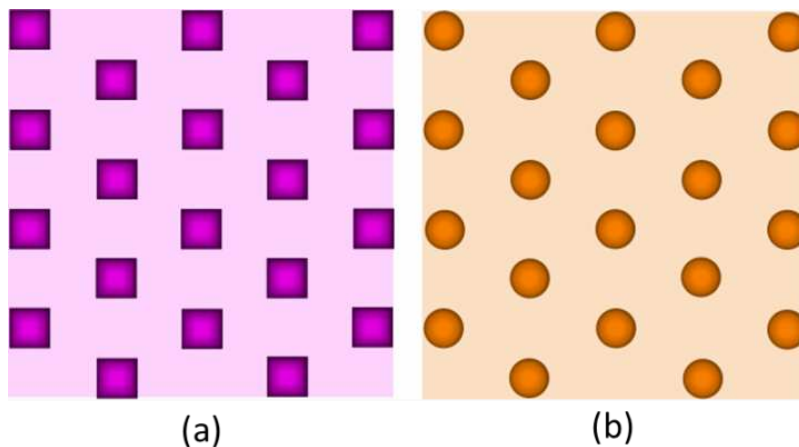


Figure 9. Examples of geometries of the 2D hexagonal lattice PC. (a) square motif (b) circular motif

### 3.2. Technique of determining light propagation direction

The direction of light propagation in any medium is given by the direction of the group velocity,  $v_g$ . Group velocity is defined as  $v_g = \nabla_{\mathbf{k}} \omega$ , where  $\nabla_{\mathbf{k}}$  is the gradient operator in the wavevector space. The light propagation direction at the frequency,  $\omega$ , can be determined using the gradient of the corresponding EFS.

Consider the problem of light of propagation from medium 1 ( $m_1$ ) to medium 2 ( $m_2$ ), as in Fig. 8. Assume  $m_1$  to be a bulk isotropic dielectric material. For a general case, assume  $m_2$  to be a 2D anisotropic PC, and for the sake of discussions, assume the anisotropic PC to be materially anisotropic. In finding the light propagation directions in  $m_2$ , there are two important orientations. These are:

- Motif orientation – All anisotropic PC have an orientation parameter (see Sec. 3.1). Let's define the orientation parameter to be an angle,  $\alpha$ . This angle defines the orientation of the motif with respect to the normal line of the interface.
- Lattice orientation – EFS of  $m_2$  is usually calculated based on a coordinate system that is aligned with one of the symmetrical axis of the lattice system [based on which the PC is constructed; examples in 2D include square lattice, rectangular lattice, honeycomb lattice, and hexagonal lattice]. This coordinate system does not necessarily align with the interface (i.e., the boundary between  $m_1$  and  $m_2$ ). This misalignment is taken into account by defining a lattice angle,  $\phi$ .

In Figure 10, we illustrate the definitions of  $\alpha$  and  $\phi$  via an example.

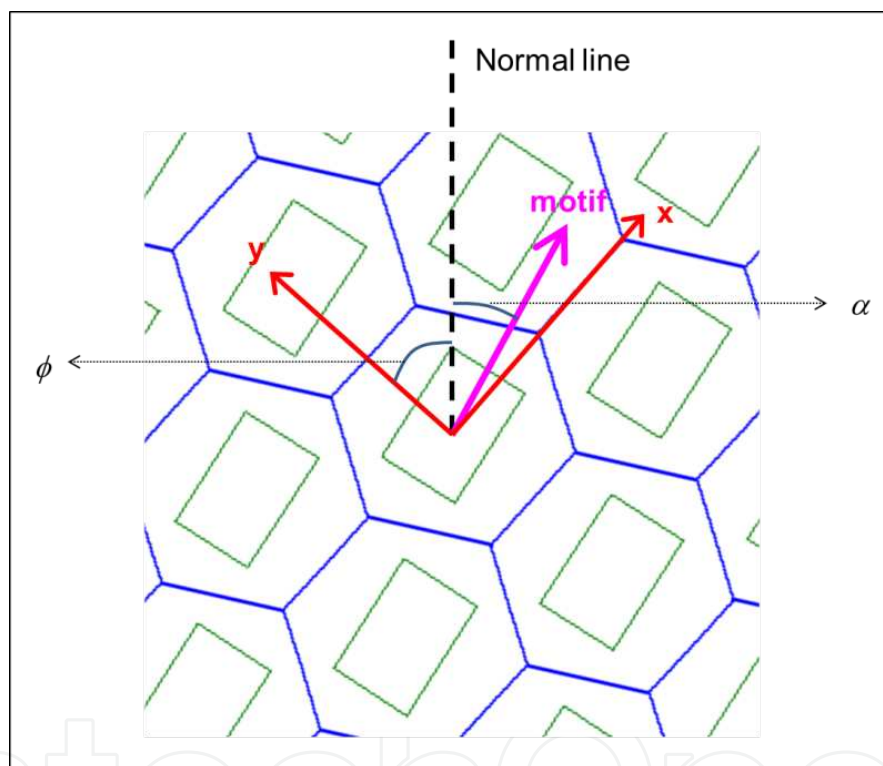


**Figure 10.** An example of  $m_2$ : A 2D hexagonal lattice PC with rectangular motifs [7]. The figure displays a microscopic view, with the details of the motif arrangement and orientation. The motifs are shown in the dark green color, while the unit cell constructions are in the blue color. The interface is normal to the dashed line (i.e., the normal line). The angle of the symmetrical axis of the motif (pink arrow) with respect to the normal line is defined as the angle of motif orientation. The angle between the symmetrical axis of the lattice (red arrows) and the normal line is defined as the lattice angle.

Figure 11(a) shows momentum space diagram that contains the EFS of the two mediums. The angles  $\alpha$  and  $\phi$  are shown in this diagram. EFS of  $m_1$  is a circle, while EFS of  $m_2$  is arbitrarily assumed. When light crosses the boundary between the two mediums, the transversal momentum (i.e., momentum component that is parallel to the interface) of light is conserved. Hence a line of momentum conservation, being a vertical line parallel to the normal line (green dashed), determined by the incident angle,  $\theta_i$ , and passing through the EFS of  $m_2$  produces

two intersection points. The directions of the normal vector at the intersection points between the EFS of  $m_2$ , and the line of momentum conservation give the propagation directions in  $m_2$ . The normal vector with the sign of the vertical component same as the sign of the incident wavevector's vertical component is considered, as a forward wave and the other, is considered as a reverse wave [Fig. 11(a)] [23]. In Fig. 11(a), the sign of  $\nabla_{\mathbf{k}}\omega$  is assumed as negative. However, take note that, depending on the sign of  $\nabla_{\mathbf{k}}\omega$ , the gradient can be either inward or outward. The consequence of such changes in the sign of  $\nabla_{\mathbf{k}}\omega$  to the directions of forward and reverse waves is illustrated in Figure 11(b).

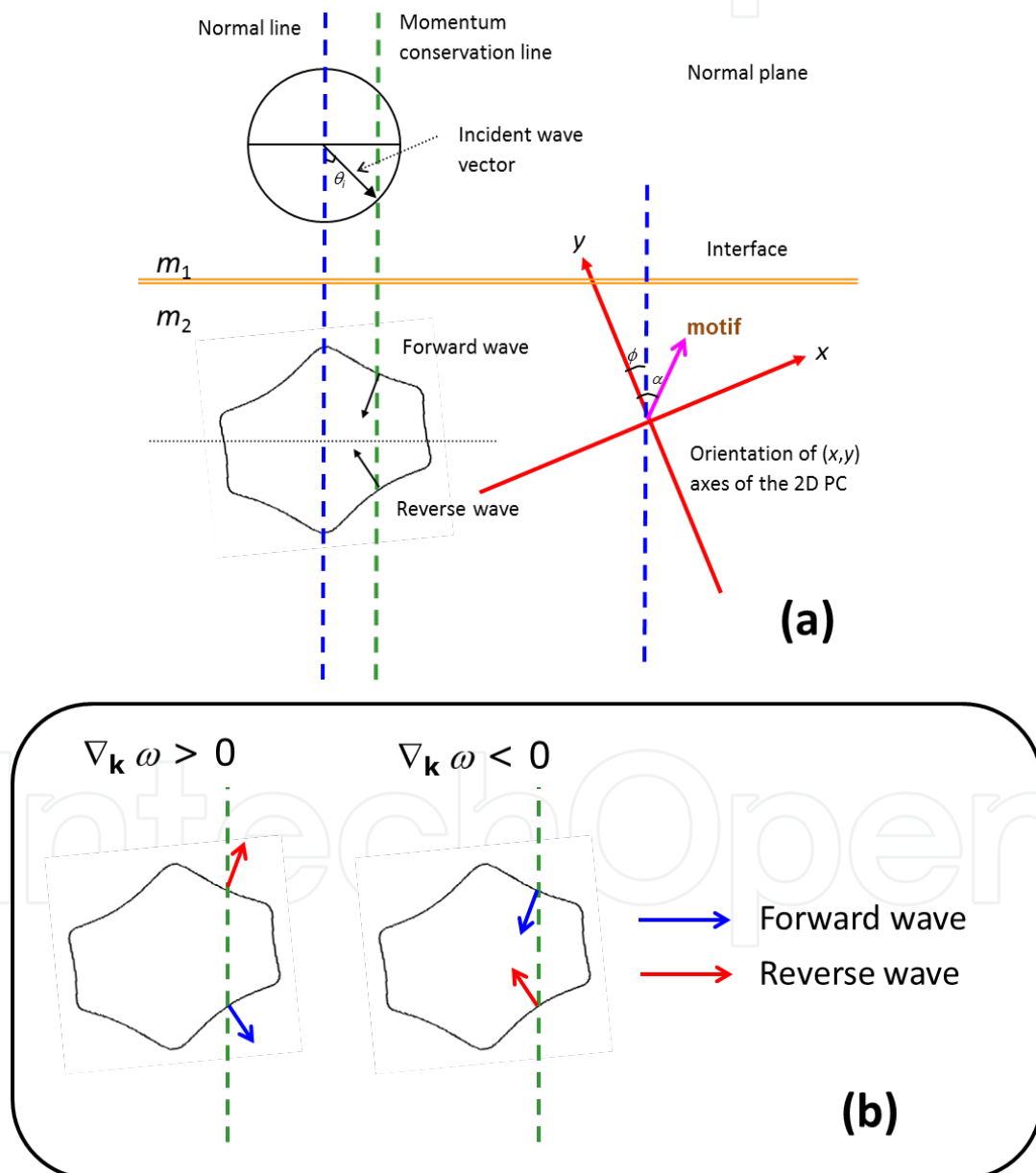


**Figure 11.** (a) In-plane propagation of light from  $m_1$  to  $m_2$ .  $m_1$ : isotropic bulk medium,  $m_2$ : anisotropic PC (b) The sign of the group velocity, and the directions of the forward and reverse waves

## 4. Applications of the EFS analysis

In this section we will use EFSs to describe few of the peculiar phenomena observed in PCs. Specifically, we will apply the concept of EFS to describe superprism, effective negative index mediums, negative refractions, and superlenses in PCs.

### 4.1. Superprism effect

Superprism effect was first demonstrated in the PC by Kosaka *et al.* [1,24]. As the name suggests, a superprism is a special and a superior version of the ordinary prism. The superprism has an extraordinary sensitivity to the incident wavelengths [24], and incident angles [1].

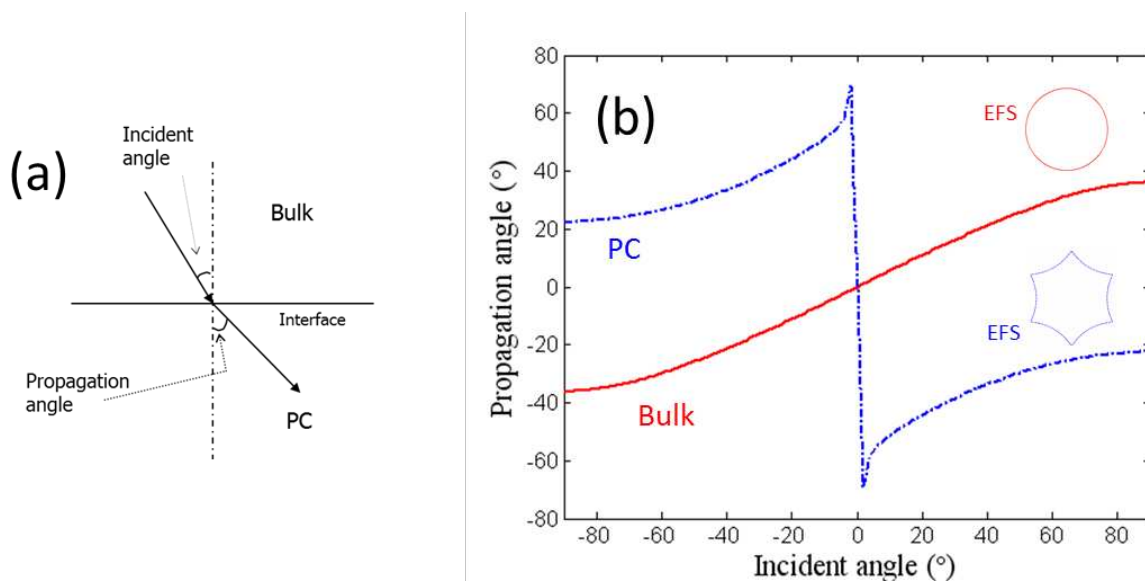
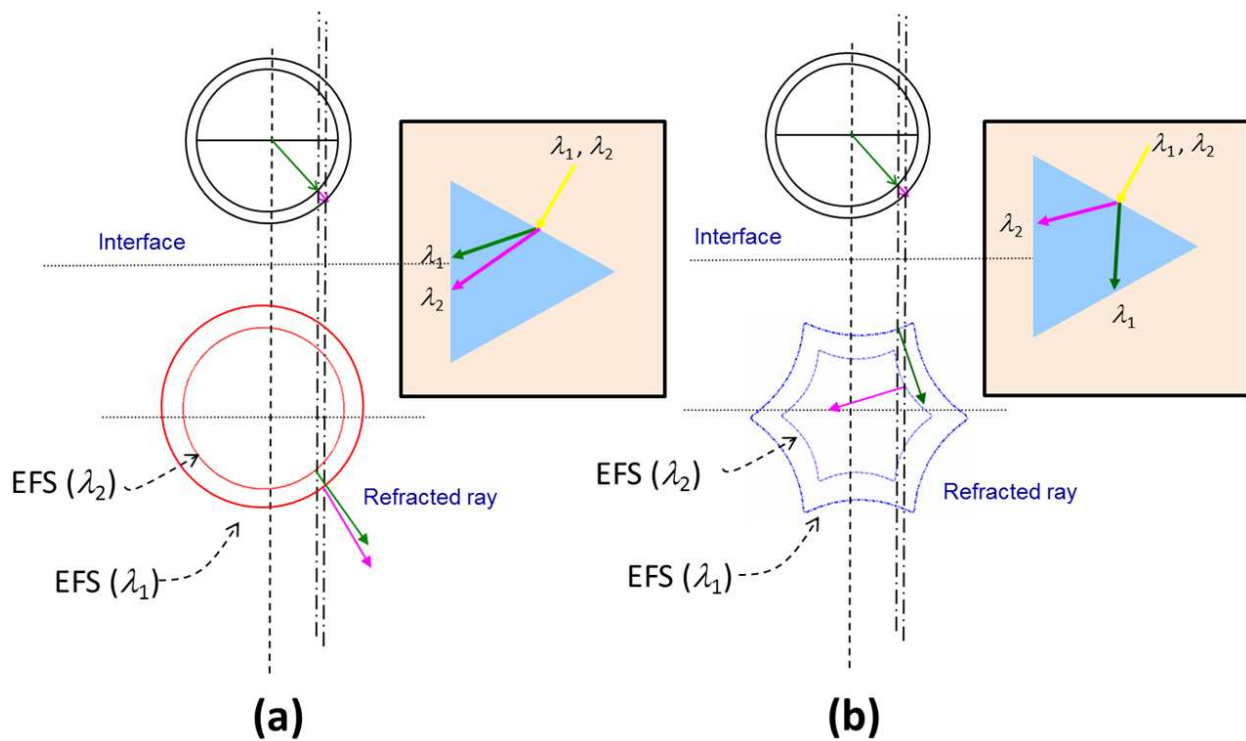


Figure 12. Angle – sensitive superprism effect

The angle sensitive superprism effect can be easily understood. In Figure 12, we show an example of the propagation angle versus incident angle plot at a specific frequency. The parameters for this plot can be found in [12]. The red curve corresponds to a bulk medium, while the blue curve is for a 2D hexagonal lattice PC. For the bulk medium, the propagation angle follows the Snell's Law, and the relationship between the incident angle and propagation angle is smooth (red curve). On the other hand, for the 2D PC, near the normal incidence, the propagation angles become highly sensitive to the incident angles (blue curve). Such a high sensitivity is due to the sharp edge observed in the corresponding hexagonal like EFS of the 2D PC [see the blue EFS in the insert].

The wavelength dependent superprism effect is useful for the spatial filtering of multiple wavelengths. Therefore, it is very useful for implementation of a compact arrayed waveguide grating [24]. The operation principle of the wavelength dependent superprism effect is graphically shown in Figure 13. Fig. 13(a) shows an ordinary prism, while Fig. 13(b) shows a superprism.



**Figure 13.** Wavelength dependent superprism effect. (a) Ordinary prism; (b) Superprism [Note that the signs of  $\nabla_{\mathbf{k}} \omega$  for the red and blue EFSs, are positives and negatives, respectively.]

Let's consider two closely spaced wavelengths,  $\lambda_1$  and  $\lambda_2$ . The EFSs for these two wavelengths are circles of different sizes in a bulk medium and in an ordinary prism. However, in a PC the EFSs can be very different. For superprism effects EFSs with sharp edges are preferred. By plotting the EFSs of the PC at various normalized frequencies ( $a/\lambda$ ), EFSs with sharp edges can be identified. Then by adjusting  $a$ , we can design the superprism at the desired wavelengths. In Fig. 13(b), example of EFSs in a 2D hexagonal lattice PC are shown. These EFSs have sharp edges, and the EFSs have different sizes. By selecting the incident angle appropriately, we can design the corresponding EFSs gradient vectors of the two wavelengths, to be at two different curvatures. As shown in Fig. 13(b), this will cause a huge difference in the propagation angles of the two closely spaced wavelengths.

#### 4.2. Effective negative index mediums

The behavior of an electron near the band edge of a semiconductor can be approximated as that of a free electron with an effective mass. The analogous concept in a PC was first shown by Notomi [2].

The EFS of a 2D PC with a symmetrical unit cell (i.e. the unit cell have a third or higher order rotational axes), becomes circular at the bottom edge of the first band (i.e., in the long wavelength limit) and for such a frequency range, the PC behaves like a bulk isotropic medium with an effective refractive index [25-26]. The effective refractive index ( $n_{eff}$ ) can be assigned by fitting the EFS to the expression  $\omega=k/|n_{eff}|$  [note that,  $\omega$  and  $k$  are normalized]. The effective

index for the first band is positive, since the first band has a positive sign of  $\nabla_{\mathbf{k}}\omega$ . It is also reported that in such 2D PCs, when the modulation of the refractive index become stronger, the EFSs become circular for frequencies near the edges of the higher order bands. Thus for the corresponding range of frequencies, the 2D PC can be homogenized to an isotropic bulk medium with an effective refractive index. However, this effective index can be negative if the sign of  $\nabla_{\mathbf{k}}\omega$  of the particular band is negative [2].

For an instance, a 2D photonic band structure of the hexagonal lattice PC with circular rods, and huge refractive index contrast is shown in Figure 14 (only the first two bands are shown) [2]. As we can see from this figure, the EFSs close to the bottom edge of the first band, and the top edge of the second band are circular. As frequency increases, the EFSs of the first band move outwards (increasing in size). Thus, the first band has a positive  $\nabla_{\mathbf{k}}\omega$ , and the corresponding circular EFSs are defined with effective positive refractive indices. On the other hand, in the second band, as frequency increases the EFSs move inwards (decreasing in size). Hence, the second band has a negative  $\nabla_{\mathbf{k}}\omega$ , and therefore their circular EFSs have effective negative refractive indices.

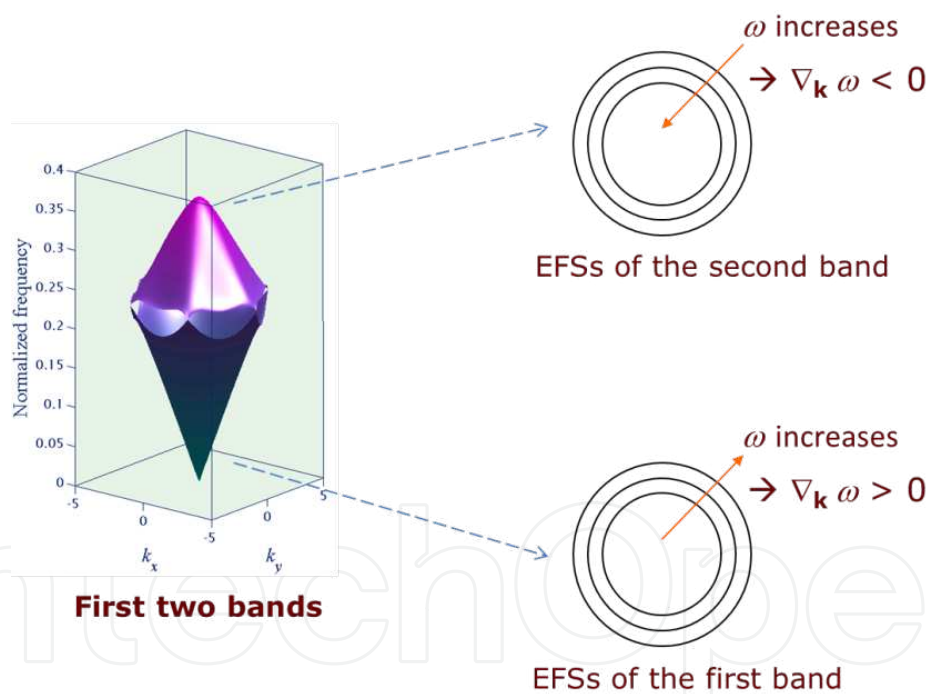


**Figure 14.** Example of circular EFSs of a PC with positive and negative effective refractive indices.

How to obtain effective anisotropic materials using PC?. Such investigations may lead to novel polarization splitting, and tunable devices.

It has been shown that, 2D materially anisotropic PCs, with symmetrically no rotational axes of order larger than two, exhibit elliptical EFSs in the long wavelength limit [25-26]. Near the higher order band edges, they do behave like a bulk anisotropic media, and if  $\nabla_{\mathbf{k}}\omega < 0$ , a set of effective negative principle refractive indices can be defined. The effective principal refractive

indices can be defined by fitting to the expression,  $\frac{k_x^2}{n_{p1}^2} + \frac{k_y^2}{n_{p2}^2} = \omega^2$ , where  $n_{p1}$  and  $n_{p2}$  are the effective principal refractive indices (note that  $\omega$ ,  $k_x$ , and  $k_y$  are normalized). As an example, in Figure 15, we show the 2D photonic band structure and the EFSs (second band) for a 2D hexagonal lattice PC with rectangular motif [7]. From this figure, we can see that, near the top edge of the second band, the EFSs are elliptical, and the signs of  $\nabla_{\mathbf{k}} \omega < 0$  (i.e., negative principal refractive indices).

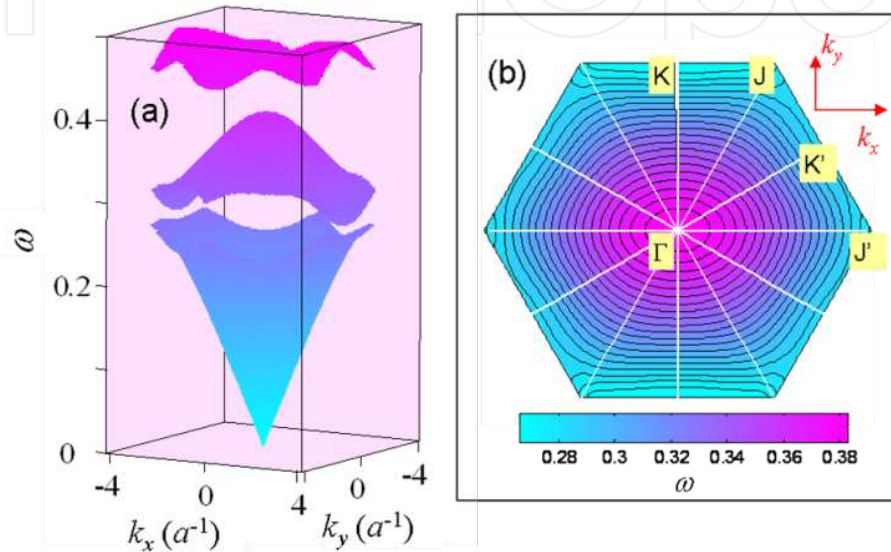


**Figure 15.** (a) 2D photonic band structure of the anisotropic PC – rectangular motif in 2D hexagonal lattice. For the details of the structure, please see [7]. (b) The contour plot of the second band in (a);

### 4.3. Negative refractions and superlenses

In the usual (positive) refraction, when light crosses the interface of the two mediums (Fig. 8), light bends on the opposite sides of the normal line. However, if light bends on the same side of the normal line, then the corresponding bending is defined as a negative refraction. Negative refraction was first predicted by Veselago in 1968 [27]. Negative refractions have been observed in artificial mediums including PCs [28-30].

For an instance of negative refraction in the PC, take a look on Figs. 12(a) and 12(b). Both incident and propagation angles in the configuration of Fig. 12(a) are defined to be positive values. If the incident (or the propagation) angle goes the other side of the normal, then it is negative. Using this formalism, it is easy to recognize that the red curve (corresponds to the bulk medium) shows propagation angles for the positive refractions, and the blue curve (corresponds to the PC) shows propagation angles for the negative refractions.

An important application of the negative refraction is a construction of a superlens [31]. Negative refraction alone does not satisfy the requirement to build a superlens. The corresponding structure also should exhibit an effective negative refractive index. Note that, a

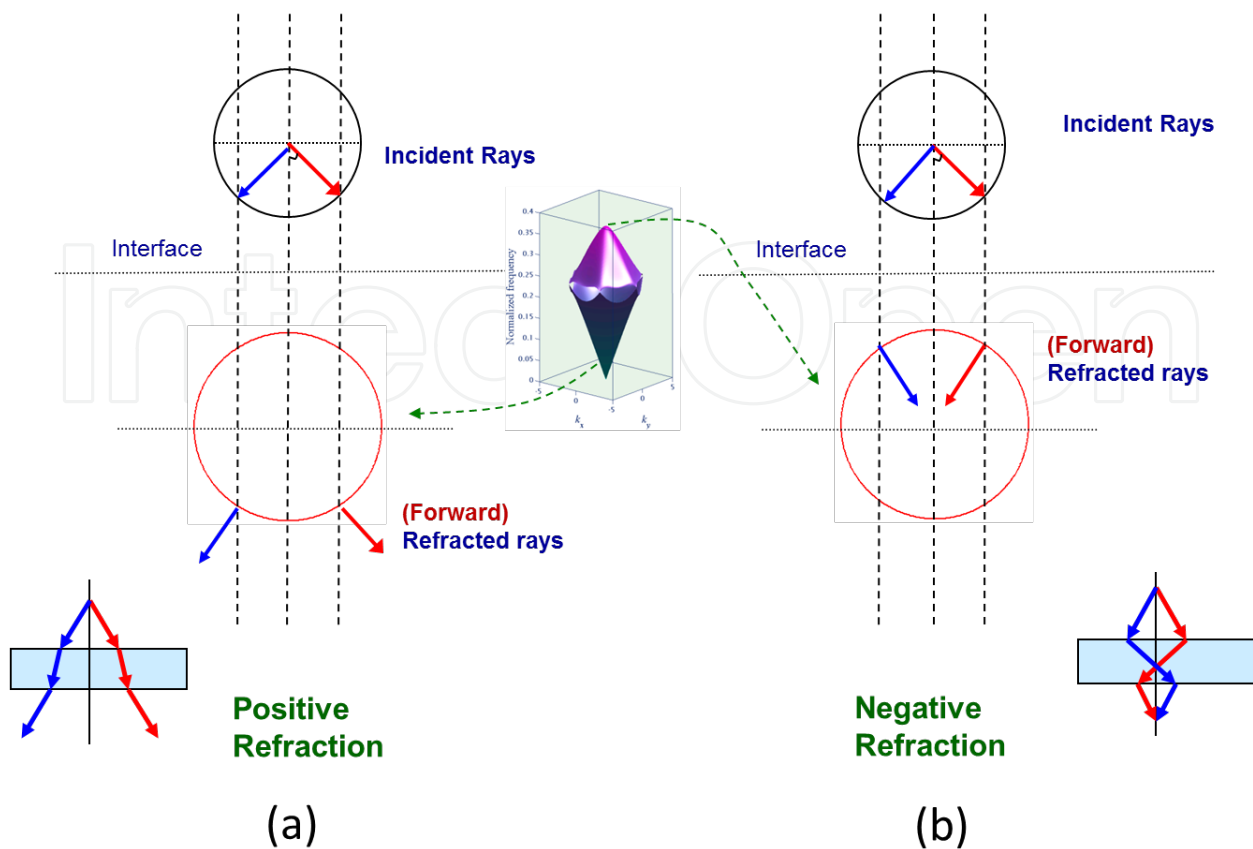


**Figure 16.** Rays from a point object (a) passing through a positive refractive index medium (b) passing through a negative refractive index medium. In both (a) and (b), the reflected rays are not shown.

negative refraction does not guarantee a negative refractive index. A effective negative refractive index ( $n_{eff}$ ) can be only defined when the EFS is circular (see Sec. 4.2). In Fig. 12(b), although we see negative refractions, the corresponding EFS (blue color) is not circular. Thus, in this case a negative refractive index cannot be defined. However, negative refractive indices can be defined for frequencies close to the top edge of the second band in Fig. 14. This frequency region has circular EFSs with  $\nabla_k \omega < 0$ .

Superlens has flat surfaces, and they produce images with subwavelength resolutions. The details on the subwavelength resolution of the superlens can be found in [31]. Here, we would like to explain, how the flat surface can result in a focusing effect. The focusing effect of the superlens is graphically illustrated in Figure 16.

Consider a homogenous slab (as in Fig. 8), and a point object at some distance from the slab in an air ambience. Firstly, assume the slab has a positive refractive index (as for the bottom edge frequencies of the first band in Fig. 14). As shown in Fig. 16, the usual positive refraction in the slab, will cause the rays from the point object to diverge. If the slab has negative refractive index (as for the top edge frequencies of the second band in Fig. 14), the negative refractions will bring the rays from the point object to a focus (see the illustration in Fig. 16(b)).

## 5. Summary

EFS is the surface resulting from the projection of the photonic band structure onto the wavevector space, at a constant frequency. In PCs, EFSs can be accurately modeled using a plane wave expansion method. For 2D PCs with weak dielectric modulation, EFSs can be obtained using one and two plane wave approximation techniques [Sec. 2]. Though one plane wave approximation succeed to a large extend in predicting the EFS of a 2D PC with a weak dielectric modulation, the approximation is inaccurate for wavevectors near the boundaries of the BZ. The one plane wave approach often predicts a very sharp edge to the EFS. The deficiencies in the one plane wave approximation is corrected in the two plane waves approach.

EFS is an essential tool in determining light propagation directions in the PC. The gradient of the EFS gives information about the group velocity direction and the sign of the propagation angle (Sec. 3). EFSs can be used to analyze various peculiar light propagations in the PC. Examples that cover superprism effects, negative index mediums, negative refractions, and superlens are discussed in Sec. 4.

## Author details

G. Alagappan\*

Address all correspondence to: [gandhi@ihpc.a-star.edu.sg](mailto:gandhi@ihpc.a-star.edu.sg)

Department of Electronics and Photonics, Institute of High Performance Computing (IHPC), Agency for Science, Technology and Research (A-STAR), Singapore

## References

- [1] Kosaka H, Kawashima T, Tomita A, Notomi M, Tamamura T, Sato T, Kawakami S. Superprism phenomena in photonic crystals. *Physical Review B* 1998; 58(16) R10096-R10099.
- [2] Notomi M. Theory of light propagation in strongly modulated photonic crystals: Refractionlike behavior in the vicinity of the photonic band gap. *Physical Review B* 2000; 62 (16) 10696-10705.
- [3] Foteinopoulou S, Soukoulis CM. Electromagnetic wave propagation in two-dimensional photonic crystals: A study of anomalous refractive effects. *Physical Review B* 2005; 72(16) 165112.

- [4] Jiang W, Chen RT, Lu X. Theory of light refraction at the surface of a photonic crystal. *Physical Review B* 2005; 71(24) 245115.
- [5] Alagappan G, Sun XW, Yu MB. Equal-frequency surface analysis of two-dimensional photonic crystals. *Journal of Optical Society of America A* 2008; 25(1) 219-224.
- [6] Alagappan G, Sun XW, Shum P, Yu MB, Engelsen D. Symmetry properties of two-dimensional anisotropic photonic crystal. *Journal of Optical Society of America A* 2006; 23(8) 2002-2013.
- [7] Alagappan G, Sun XW, Yu MB. Negative principal refractive indices and accidental isotropy in two dimensional photonic crystals with an asymmetrical unit cell. *Physical Review B* 2007; 76(16) 165123.
- [8] Ho KM, Chan CT, Soukoulis CM. Existence of a photonic gap in periodic dielectric structures. *Physical Review Letters* 1990; 65(25) 3152-3155.
- [9] Sakoda K. *Optical Properties of Photonic Crystals*. Berlin: Springer; 2005.
- [10] Li MS, Wu ST, Fuh AYG. Superprism phenomenon based on holographic polymer dispersed liquid crystal films. *Applied Physics Letters* 2006; 88(9) 91109.
- [11] Baumberg JJ, Perney NMB, Netti MC, Charlton MDC, Zoorob M, Parker GJ. Visible-wavelength super-refraction in photonic crystal superprisms. *Applied Physics Letters* 2004; 85(3) 354-356.
- [12] Alagappan G, Sun XW, Shum P, Yu MB. Tunable superprism and polarization splitting in a liquid crystal infiltrated two-dimensional photonic crystal made of silicon oxynitride. *Optics Letters* 2006; 31(8) 1109-1111.
- [13] Liu YJ, Sun XW. Electrically tunable two-dimensional holographic photonic crystal fabricated by a single diffractive element. *Applied Physics Letters* 2001; 89(17) 171101.
- [14] Harrison WA. Fermi Surface in Aluminum. *Physical Review* 1959; 116(3) 555-561.
- [15] Ziman JM. *Principles of the Theory of Solids*. Cambridge: Cambridge University Press; 1972.
- [16] Busch K, John S. Photonic band gap formation in certain self-organizing systems. *Physical Review E* 1998; 58(3) 3896-3908.
- [17] Busch K, John S. Liquid-Crystal Photonic-Band-Gap Materials: The Tunable Electromagnetic Vacuum. *Physical Review Letters* 1999; 83(5) 967-970.
- [18] Liu CY, Chen LW. Tunable band gap in a photonic crystal modulated by a nematic liquid crystal. *Physical Review B* 2005; 72(4) 045133.
- [19] Alagappan G, Sun XW, Shum P, Yu MB. Engineering the band gap of a two-dimensional anisotropic photonic crystal. *Journal of Optical Society of America B* 2006; 23(7) 1478-1483.

- [20] Takeda T, K. Yoshino. Tunable refraction effects in two-dimensional photonic crystals utilizing liquid crystal. *Physical Review E* 2003; 67(5) 056607.
- [21] Gasiorowicz S. *Quantum Physics*. John Willey & Sons; 2003.
- [22] Alagappan G, Sun XW, Sun HD. Symmetries of the eigenstates in an anisotropic photonic crystal. *Physical Review B* 2008; 77(19) 195117.
- [23] Baba T. Photonic crystal light deflection devices using the superprism effect. *IEEE Journal of Quantum Electronics* 2002; 38(7) 909-914.
- [24] Kosaka H, Kawashima T, Tomita A, Notomi M, Tamamura T, Sato T, Kawakami S. Photonic crystals for micro lightwave circuits using wavelength-dependent angular beam steering. *Applied Physics Letters* 1999; 74(10) 1370-1372.
- [25] Halevi H, Krokhin AA, Arriaga A. Photonic Crystal Optics and Homogenization of 2D Periodic Composites. *Physical Review Letter* 1999; 82(4) 719-722.
- [26] Krokhin AA, Halevi P, Arriaga J. Long-wavelength limit (homogenization) for two-dimensional photonic crystals. *Physical Review B* 2002; 65(11) 115208.
- [27] Veselago VG. The electrodynamics of substances with simultaneously negative values of  $\epsilon$  and  $\mu$ . *Soviet Physics Uspekhi* (1968);10(4) 509–514.
- [28] Shelby RA, Smith DR, Schultz S. Experimental Verification of a Negative Index of Refraction. *Science* 2001; 292(5514) 77-79.
- [29] Berrier A, et al. Negative Refraction at Infrared Wavelengths in a Two-Dimensional Photonic Crystal. *Physical Review Letters* 2004, 93(7) 073902 (2004).
- [30] Schonbrun E, et al. Negative-index imaging by an index-matched photonic crystal slab. *Physical Review B* 73(19), 195117 (2006).
- [31] Pendry JB. Negative Refraction Makes a Perfect Lens. *Physical Review Letters* 2000; 85(18) 3966-3969.

IntechOpen